The final publication is available at

https://doi.org/10.1039/c6dt00370b

Additional Information

Multinuclear Silver(I) XPhos Complexes with Cyclooctatetraene: Photochemical C-C bond cleavage of Acetonitrile and Cyanide bridged Ag clusters formation

Abdessamad Grirrane,*[a] Eleuterio Álvarez,[b] Josep Albero,[a] Hermenegildo García,*[a] and Avelino Corma*[a]

[a]	Dr. A. Grirrane, Dr. J. Albero, Prof. Dr. H. Garcia, Prof. Dr. A. Corma Instituto Universitario de Tecnología Química CSIC-UPV Universidad Politécnica de Valencia Av. De los Naranjos s/n, 46022 Valencia (Spain) Fax: (+34) 963877809 E-mail: hgarcia@qim.upv.es, acorma@itq.upv.es, grirrane@itq.upv.es,
[b]	Dr. E. Álvarez Instituto de Investigaciones Químicas IIQ-CSIC-US Consejo Superior de Investigaciones Científicas - Universidad de Sevilla. Av. Américo Vespucio 49, 41092 Sevilla (Spain). E-mail: ealvarez@iiq.csic.es

Supporting information for this article is given via a link at the end of the document.

Abstract: Cationic mono-, di-, tri- and tetra-nuclear silver complexes with Buchwald-type phosphane (XPhos) and cyclooctatetraene (COT) have been synthesized and characterized. Formation of $[(XPhos-Ag)_n(COT)][SbF_6]_n$ (n = 1 and 2) complexes was confirmed by single-crystal X-ray crystallography and multinuclear NMR spectroscopy. Variable-temperature NMR spectroscopy in CD_2Cl_2 solution shows the fluxionality of COT ring in mono- Ag(I) XPhos complex. Fluxionality of COT was also confirmed in the case of di- Ag(I) XPhos complex by solid-state and solution ^{31}P NMR spectroscopy. The C-C bond cleavage of coordinated acetonitrile [XPhos-Ag(I)-NCCH₃] resulting in cyanide bridged Ag clusters formation $[(XPhos-Ag)_2(\mu-CN)_n(\mu-Ag)_{n-1}]$ (n = 1, 2, 3 and 4) upon light excitation of $[(XPhos-Ag)_n(COT)]$ was confirmed by HRESI-MS, UV-Absorption and HR-TEM.

Chemistry of mono- and multi- nuclear sandwich complexes has developed extensively,[1-6] since ferrocene was discovered.[7, 8] Silver is widely used due to its coordination modes[9-11] and its affinity for hard donor atoms such as nitrogen or oxygen.[12] Due to their general interest, complexes between Ag(I) metal ions and π-bonding systems of unsaturated or conjugated organic compounds have received experimental[13-15] and theoretical[12, 16, 17] attention. The preparation of Ag(I)-cyclooctatetraene (COT) complex[15] has been previously reported and the interaction between Ag(I) ion and C≡C double bond elucidated. Herein, four new cationic Ag(I) complexes between bulky 2-di-tert-

butylphosphanylbiphenyl (XPhos)[18] with COT ligand have been synthesized and characterized. The consecutive mono- di-, tri- and tetra- XPhos-Ag(I) complexes with COT are described. Fluxionality and coordination mode of COT ligand in Xphos-Ag(I) complexes were confirmed and studied by variable-temperature NMR spectroscopy and single-crystal X-ray crystallography. The interaction between Ag(I) ion and C=C double bond of COT ring and Ag-C_{arene} interaction in these Xphos complexes have been compared with analogous Cu- and Au-C_{arene} interaction present in similar Xphos complexes,[19-22] thus showing the influence of the metal on the metal-arene interaction. Laser irradiation of cationic $[(XPhos-Ag)_n(COT)][SbF_6]_n$ (n = 1, 2, 3 and 4) complexes in acetonitrile leads to cleavage of the C-C bond of coordinated acetonitrile in Xphos-Ag(I)-($NCCH_3$) adduct initially formed by solvent exchange of COT ligand inducing in the first stage the formation a cyanide bridged dinuclear $[(XPhos-Ag)_2(\mu-CN)]$ complex followed by formation of a tri-, tetra- and penta- nuclear $[(XPhos-Ag)_2(\mu-CN)_n(\mu-Ag)_{n-1}]$ (n = 2, 3 and 4) clusters by addition, respectively, of one, two and three [Ag-CN] fragments over a cyanide bridged $[(XPhos-Ag)_2(\mu-CN^-)]$. Our study shows remarkable catalytic activity of Xphos-Ag(I) complexes for selective photochemical C-C bond cleavage[23-28] of acetonitrile and the controlled evolution of XPhos-Ag(I) complexes leading to the formation of well defined Ag clusters as confirmed by HRESI-MS and HR-TEM images.

In the initial stage of our study, we selected $[Ag]^+[SbF_6]^-$ salt as precursor for the preparation of cationic Ag(I) dialkylbiarylphosphane complexes **1** and **2** (Scheme 1). The reaction of a (1:1:1) or (2:2:1) stoichiometric mixture of $AgSbF_6$, 2-di-tert-butylphosphanylbiphenyl (Xphos) and COT in CH_2Cl_2 at room temperature for 24 h (Scheme 1), filtration of the resulting transparent pale yellow solutions, followed by addition of n-hexane at -8 ºC and -2 ºC, respectively, leads to the formation of cationic Ag(I) complexes $[Xphos-Ag(\eta^4-COT)][SbF_6]$ (**1**) and $[(Xphos-Ag)_2 \ \mu_2-(\eta^4:\eta^2-COT)][SbF_6]_2$ (**2**) in 94 % and 92 % yield, respectively [See the Experimental Section in the Supporting Information (ESI)].

Complexes **1** and **2** were fully characterised by analytical data, NMR spectroscopy, ESI-MS, combustion elemental analysis. In both complexes **1** and **2**, the solid state structure was confirmed by single-crystal X-ray crystallography and the fluxional behaviour of COT ring in the case of complex **1** was studied by variable-temperature NMR spectroscopy.
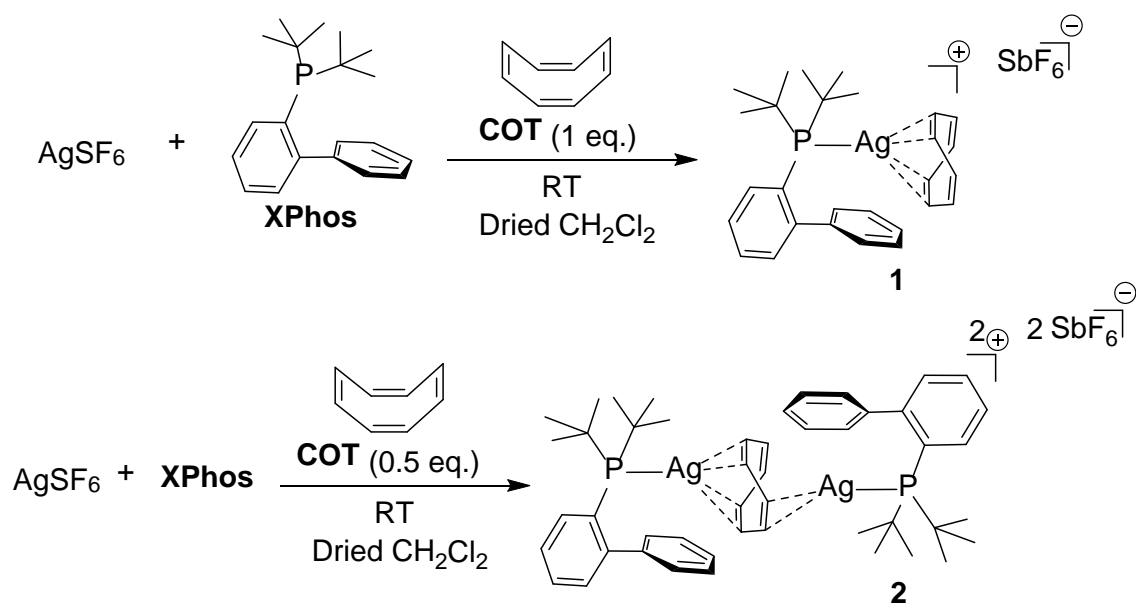
Scheme 1. Synthesis of cationic mono- and di-Ag(I) complexes **1** and **2** in dried CH_2Cl_2 at room temperature by simultaneous addition of reagents $AgSbF_6$, XPhos and COT in the corresponding 1:1:1 and 2:2:1 stoichiometry, respectively.

Structural data obtained by X-ray diffraction of complex **1** (Figure 1, top) show a cationic monometallic structure, with a bent COT ring coordinated to the Ag^+ ion in $\eta^2:\eta^2$ manner to non-adjacent "π" double bonds of COT. The nearest carbon atom neighbours of the silver atom are C21 and C22, respectively at an average distance of 2.465 (4) and 2.432 (4) Å, followed by C25 and C26 respectively at an average distance of 2.921 (4) and 2.972 (5) Å. Coordination sphere of Ag is completed by P atom from phosphine ligand (XPhos) with an average distance of 2.4137 (11) Å and Ag-flanking arene interactions at an average distance of 2.910 Å for Ag-C(7)$_{ipso}$ and the distance between Ag and the closest carbon atom (C12) of the distal phenyl ring at an average distance of 2.872 Å (see Table S1 and Fig. S1 in ESI for full details of the crystallographic data). The crystal packing details of **1** viewed along the a-axis shows the presence of inter- and intramolecular hydrogen bonds of F atoms of SbF_6 counteranion with H atoms from tert-butyl group, COT ring and central phenyl ring (Fig. S1 in the ESI). The solid state structure of this new cationic Ag(I) complex **1** is closely related to that of our recently reported solid state structures of cationic Ag(I) complexes (XPhos-aniline-Ag^I)[19] and (XPhos-pyrrolidine-Ag^I)[19] having amine instead of COT ligand and presenting comparable distances between Ag ion and its coordination sphere. The distances Ag-N,

3

Ag-P, Ag-C(7)$_{ipso}$ and the distance between Ag and the closest carbon atom (C12) of the distal phenyl ring in Ag(I) complexes are, on the other hand, longer compared with a closely related, previously reported PF$_6^-$ salt of Cu^I analogues (XPhos-aniline-Cu^I)[20] and (XPhos-pyrrolidine-Cu^I)[20, 21]. Our previous published cationic XPhos-aniline-Au(I) complex[22] present intermediate bond lengths for Au-N(1) and Au-P(1) compared to the silver and copper analogues. Thus, analysis of bond lengths in the crystal structure shows the influence of the metal (Cu, Ag and Au) on the metal-arene interaction, the case of XPhos-Ag(I) being the complex with longest distances, indicating a weaker interaction compared to Cu(I) and Au(I).
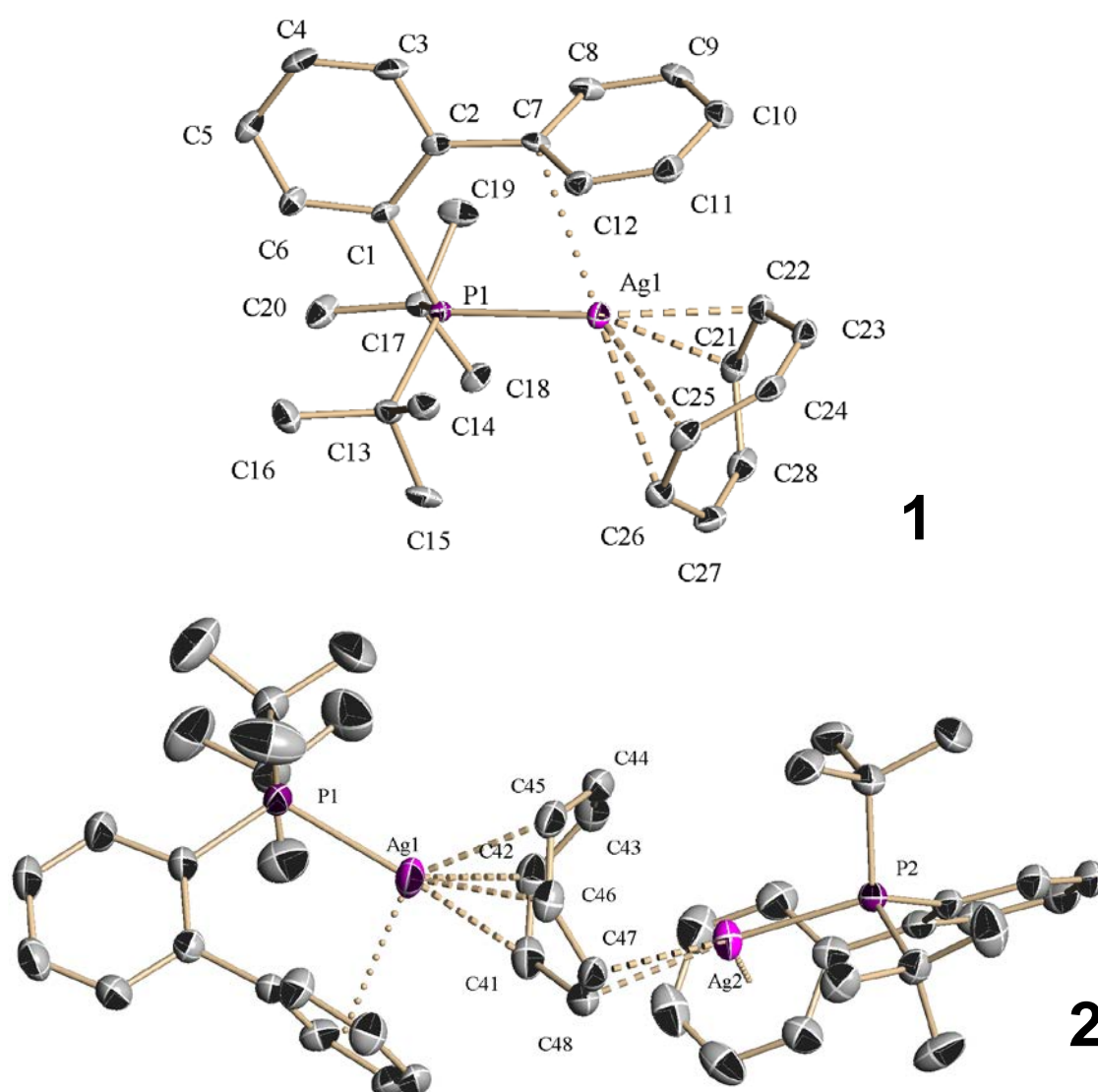
Figure 1. ORTEPS view of the solid-state structures of complexes **1** and **2**; ellipsoids are given at the 30 % probability level (counteranion and C-H hydrogen atoms were omitted for clarity). Single-crystal X-ray data and crystal packing details are given, respectively, for **1** and **2** in Table S1, Fig.S1 and Table S2, Fig.S9 in the ESI).

The silver (I) complex **1** was also characterized by NMR spectroscopy and ESI-MS. ^{1}H, ^{13}C, DEPT and ^{31}P NMR spectra in CD_2Cl_2 providing evidence that the starting AgSbF$_6$ salt was completely converted into **1** (see Figs. S2-S8 in the ESI). Thus, the formation of a Ag-P bond in complex **1** is firmly confirmed by the appearance in ^{31}P NMR spectroscopy of two doublets due to coupling of ^{31}P with the two silver isotopes (^{107}Ag and ^{109}Ag) both of spin ½ at 42.01 ppm with $^1J(^{107}$Ag-^{31}P$) = $ 573.98 Hz and $^1J(^{109}$Ag-^{31}P$) = $ 662.38 Hz (see Fig. S5 in the ESI). Similarly, ^{1}H NMR spectroscopy showed new signals for the methyl groups of complex **1** at 1.28 and 1.23 ppm (see Fig. S2 in the ESI) instead of those corresponding to the initial free phosphine ligand (XPhos) at 1.11 and 1.07 ppm. NMR data of **1** is consistent with fluxional behaviour of the COT unit. A single resonance was found for COT both ^{1}H and the ^{13}C{^{1}H} NMR spectra at δ = 5.98 ppm and 132.6 ppm, respectively (CD_2Cl_2) (See Figure 2 (a) and (c), additional details in Fig. S2 and S3 in the ESI), indicating the fast exchange of Ag$^+$ with the "π"-bonds of COT from C21=C22 and C25=C26 to C23=C24 and C27=C28 (see Figure 1, ORTEP of **1**). This exchange rate was sufficiently slowed down at low temperature (-80 ºC, CD_2Cl_2), resulting, then, in two signals at δ = 5.96; 5.93 ppm and 132.8; 132.1 ppm, respectively, for ^{1}H and the ^{13}C{^{1}H} NMR spectra (See Figure 2 (b) and (d), additional details in Figs. S7 and S8 in the ESI).

ESI-MS of a solution obtained after dissolving complex **1** in CH_2Cl_2/CH_3CN shows mainly a series of peaks with major positive MS peaks at 405.1 and 407.1 Da attributable to cationic Ag(I) complex with the ^{107}Ag and ^{109}Ag isomers of $[C_{28}H_{35}AgF_6PSb$ (**1**) - SbF$_6^-$ and - C_8H_8 ring$]^+$ and other series with major positive MS peaks at 549.1 Da attributable to cationic Ag(I) complex with the ^{107}Ag and ^{109}Ag isomers of $[C_{28}H_{35}AgF_6PSb$ (**1**) - SbF$_6^-$ and + K$]^+$ (see Fig. S6 in the ESI). In negative MS mode the presence of peaks at 234.8 and 236.9 Da attributable to SbF$_6^-$ counter-anion of complex **1** with the corresponding ^{121}Sb and ^{123}Sb isotopic distribution was also observed (see Fig. S6 in the ESI).
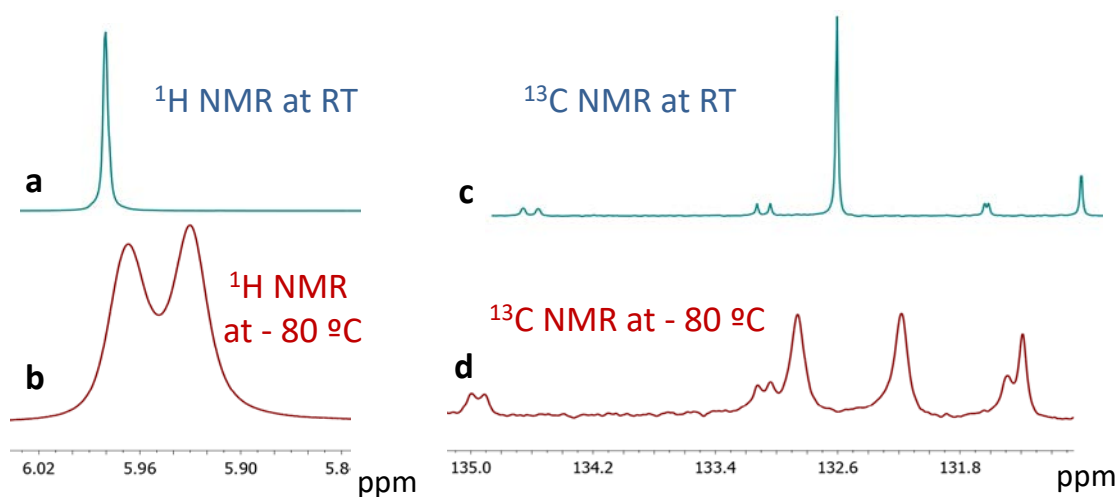
Figure 2. ^{1}H (**a**, **b**) and ^{13}C (**c**, **d**) NMR spectra of complex **1** [NMR spectra at 25 °C (**a**, **c**) and at -80 °C (**b**, **d**)]. (see Figs. S2-S3 and S7-S8 in the ESI for additional details).

On the other hand, the structural data obtained by single-crystal X-ray diffraction of complex **2** (Figure 1, bottom) shows a di-cationic bimetallic structure, with a bent COT ring unsymmetrically bridging the two Ag^{+} ions in opposite sides of COT ring having approximate η^{2}:η^{4} manner with non-adjacent "π" double bonds, the crystal structure of solid complex **2** being in agreement with analytical data,^{1}H, ^{13}C and ^{31}P NMR spectra and ESI-MS. Isolation of **2** shows that the reaction with a 2:1:2 stoichiometry XPhos, COT, AgSbF$_{6}$ has proceeded with the coordination of two Ag^{+} ions in the non-planar geometry expected for a 8 π antiaromatic ring.[29]

The solid state structure of the cationic bis-Ag inverse sandwich complex [(XPhos-Ag)$_{2}$ μ$_{2}$-(η^{4}:η^{2}-COT)][SbF$_{6}$]$_{2}$ (**2**) (Figure 1, bottom) shows that the nearest carbon atoms of COT to the Ag1 ion (η^{4} bonding form) are C45 and C46 of a double bond, respectively at an average distance of 2.596 (4) and 2.614 (4) Å, followed by C41 and C42 of the other double bond respectively at an average distance of 2.677 (4) and 2.690 (4) Å. The coordination sphere of Ag1 is completed by P1 atom from XPhos ligand with an average distance of 2.4281 (11) and Ag-flanking arene interaction (C7$_{ipso}$) at an average distance of 2.944 Å. The second Ag atom, Ag2, shows a different bonding pattern (η^{2} bonding form) with the nearest carbon atom of COT bridged to the Ag2 atom being C47 and C48 of a double bond with an average distance of 2.490 (4) and 2.442 (4) Å respectively, that is significantly shorter compared with the Ag1-C(COT) distances. The

coordination sphere of Ag2 is completed by P2 atom from the second XPhos ligand with very similar distances as Ag1-XPhos with an average distance of 2.4303 (10) and Ag-flanking arene interaction (C27$_{ipso}$) at an average distance of 2.992 Å (for details, see Fig.S9 and Table S2 in ESI).

The Ag(I) complex **2** was also characterized by ^{1}H, ^{13}C, DEPT and ^{31}P NMR spectroscopy, ESI-MS and combustion analysis (see the experimental section and Figs. S10-S14 in the ESI). ^{1}H, ^{13}C, DEPT and ^{31}P NMR spectra in CD$_2$Cl$_2$ provided evidence that the starting AgSbF$_6$ (**1**) salt was completely converted into **2** (see Figs. S10-S13 in the ESI). Thus, the formation of a Ag-P bond in complex **2** is firmly confirmed by the appearance in ^{31}P NMR spectroscopy of the signals corresponding to a single type of P consisting in two doublets due to coupling of ^{31}P with the two Ag isotopes (^{107}Ag and ^{109}Ag) both of spin ½ at the same chemical shift 43.54 ppm with $^1J(^{107}$Ag-^{31}P) = 626.58 Hz and $^1J(^{109}$Ag-^{31}P) = 723.63 Hz (see Fig. S13 in the ESI). Similarly, ^{1}H NMR spectroscopy showed a shift in the chemical shift for the methyl groups of complex **2** at 1.29 and 1.23 ppm (see Fig. S10 in the ESI) with respect to those corresponding to the initial free phosphine ligand (XPhos) at 1.11 and 1.07 ppm. ESI-MS of a solution obtained after dissolving complex **2** in CH$_2$Cl$_2$ shows mainly a series of peaks with major positive MS peaks at 938.9 Da attributable to cationic Na$^+$ [XPhos-Ag]$_2$(COT) complex with the ^{107}Ag and ^{109}Ag isomers of [C$_{48}$H$_{62}$Ag$_2$F$_{12}$P$_2$Sb$_2$ (**2**) - 2SbF$_6^-$ and + Na]$^+$ (Fig. S14 in the ESI). The measured mass distribution was in good agreement with the simulated isotopic distribution for [C$_{48}$H$_{62}$Ag$_2$P$_2$Na]$^+$ (see details in Fig. S14 in the ESI). Other smaller series of ions with major positive peaks at 847.0 Da attributable to cationic Ag(I) complex [C$_{48}$H$_{62}$Ag$_2$F$_{12}$P$_2$Sb$_2$ (**2**) - 2SbF$_6^-$ - COT and + Cl]$^+$ with the ^{107}Ag and ^{109}Ag isotopes (see Fig. S14 in the ESI) was also observed, suggesting that under these conditions some CH$_2$Cl$_2$ was reacted, releasing chloride to form some neutral dichloride-bridged disilver (I) complex [L-Ag(μ-Cl)]$_2$ characterized previously by us.[19] If one chlorine atom is lost the major positive MS peaks would appear at 847.2 Da. The fragmentation of this cluster of peaks is in agreement with the proposed composition (see Fig. S14 in the ESI).

Having isolated the dicationic Ag(I)$_2$ complex **2**, it was of interest to determine the capability of COT ligand to coordinate with more than two [Ag-XPhos] fragments. Accordingly, a new set of reactions were carried out, in which stoichiometric (3:3:1) and (4:4:1) mixtures of AgSbF$_6$, XPhos and COT were stirred in CH$_2$Cl$_2$ at room temperature for 24 h (Scheme 2), filtering the resulting transparent pale yellow solutions, followed by

addition of n-hexane at -8 ºC. This procedure led to the formation of cationic tri- and tetra- Ag(I) complexes [(XPhos-Ag)$_3$(μ_3-COT)][SbF$_6$]$_3$ (**3**) and [(XPhos-Ag)$_4$(μ_4-COT)][SbF$_6$]$_4$ (**4**) in 90 and 92 % yields, respectively. Unfortunately in both cases single crystals of complexes **3** and **4** with sufficient size to resolve their structures by solid state X-ray crystallography could not be obtained and complexes **3** and **4** were characterised exclusively by ^{1}H, ^{13}C, DEPT and ^{31}P NMR spectroscopy, ESI-MS and combustion elemental analysis (See the Experimental Section and Figs. S15-S23 in the ESI)

^{1}H, ^{13}C, DEPT and ^{31}P NMR spectra in CD$_2$Cl$_2$ provided evidence that the starting AgSbF$_6$ salt was completely converted into **3** and **4** depending on the stoichiometry of the reagents (see Figs. S15-S18 for **3** and Figs. S19-S22 for **4** in the ESI). Thus, the formation of a Ag-P bond in complexes **3** and **4** was firmly confirmed by the appearance in ^{31}P NMR spectroscopy of two doublets due to coupling of ^{31}P with the two Ag isotopes (^{107}Ag and ^{109}Ag) both of spin ½, respectively, at chemical shifts 44.82 and 45.21 ppm for both complexes with $^1J(^{107}$Ag-^{31}P) = 670.40 Hz, $^1J(^{109}$Ag-^{31}P) = 773.86 Hz and $^1J(^{107}$Ag-^{31}P) = 682.47 Hz, $^1J(^{109}$Ag-^{31}P) = 788.01 Hz for complexes **3** and **4**, respectively (see Fig. S18 for **3** and Fig. S22 for **4** in the ESI). ESI-MS of a solution obtained after dissolving tetra- Ag(I) [(XPhos-Ag)$_4$(μ_4-COT)][SbF$_6$]$_4$ (**4**) complex in CH$_2$Cl$_2$/toluene shows a small series of peaks with major positive MS peaks at 1347.5 Da attributable to cationic Na$^+$ [(XPhos-Ag)$_3$(μ_3-COT)] complex with the ^{107}Ag and ^{109}Ag isomers of complex [(XPhos-Ag)$_3$(μ_3-COT)][SbF$_6$]$_3$ (**3**) - 3SbF$_6$$^-$ and + Na]$^+$ (see details in Fig. S23 in the ESI) and an additional series with major positive MS peaks at 938.9 and 838.0 Da attributable to cationic Na$^+$ bis-[XPhos Ag(I)]-COT complex with the ^{107}Ag and ^{109}Ag isotopes of [C$_{48}$H$_{62}$Ag$_2$F$_{12}$P$_2$Sb$_2$ (**2**) - 2SbF$_6$$^-$ and + Na]$^+$ and when this fragment lose a COT ring also observed above for complex **2** (see Fig. S23 in the ESI).
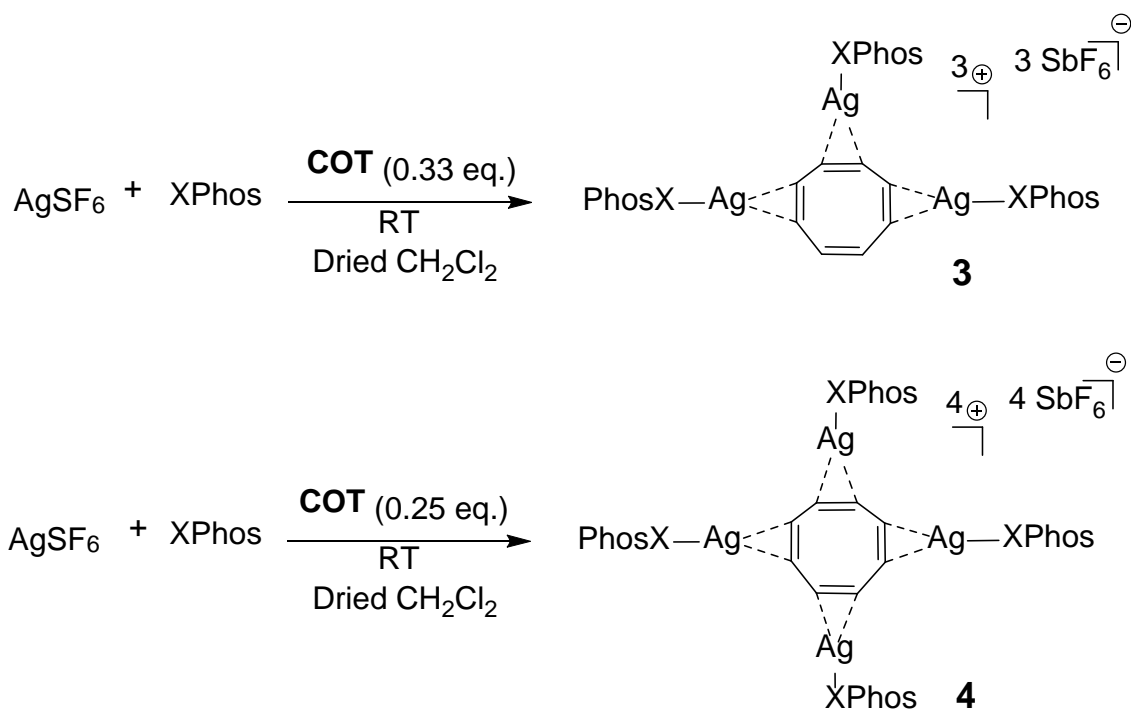
Scheme 2. Synthesis of cationic tri- and tetra-Ag(I) complexes **3** and **4** in dried CH_2Cl_2 at room temperature by simultaneous addition of $AgSbF_6$, XPhos and COT in the corresponding stoichiometry 1:1:0.33 and 1:1:0.25, respectively.

Attempts to record solid state ^{31}P NMR spectra of complex [(XPhos-Ag)$_2$ μ_2-(η^4:η^2-COT)][SbF$_6$]$_2$ (**2**) obtained by fast evaporation of its corresponding mother liquid at 24 h reaction times, in which complex **2** should have been formed due to the 2:2:1 stoichiometry of $AgSbF_6$, XPhos and COT met with failure resulting in the solid state ^{31}P NMR spectrum shown in Figure 3 (bottom:**b**) (For details see: Fig.S26 in the ESI) corresponding to a complex mixture of complexes. Analysis of this solid state ^{31}P NMR spectrum showed that it was a combination of the solid state ^{31}P NMR spectra of complexes **1** and **4** with additional peaks attributable to complexes **2** and **3**. Thus, when the solid state ^{31}P NMR spectroscopy for the crude solids of complexes **1** and **4** obtained by fast evaporation of their corresponding mother liquid at 24 h reaction time was also recorded independently, the combination of both agrees with the one recorded for the attempted solid state ^{31}P NMR spectra of **2**. Solid state ^{31}P NMR spectra for the compounds **1** [Figure 3, bottom (**a**) and Fig. S24 in the ESI] and **4** [Figure 3, bottom (**c**) and Fig. S25 in the ESI] were in agreement with the corresponding ^{31}P NMR spectra for these complexes in CD_2Cl_2 solution (see, respectively, Fig. S5 and Fig. S22 in the ESI).

9

In solid state the ^{31}P peak of complex **1** appears at 42.03 ppm as a pair of doublets [$^1J(^{107}Ag-^{31}P)$ = 566.7 Hz, $^1J(^{109}Ag-^{31}P)$ = 639.9 Hz] (see Fig.S24 in the ESI). In the case of complex **4** the ^{31}P peak in CD_2Cl_2 solution and in solid state appears, respectively, at 45.21 ppm as a pair of doublets [$^1J(^{107}Ag-^{31}P)$ = 682.5 Hz, $^1J(^{109}Ag-^{31}P)$ = 788.0 Hz] (see Fig.S22 in the ESI) and at 45.59 ppm as a pair of doublets (see Fig.S25 in the ESI) [$^1J(^{107}Ag-^{31}P)$ = 728.67 Hz, $^1J(^{109}Ag-^{31}P)$ = 830.42 Hz].
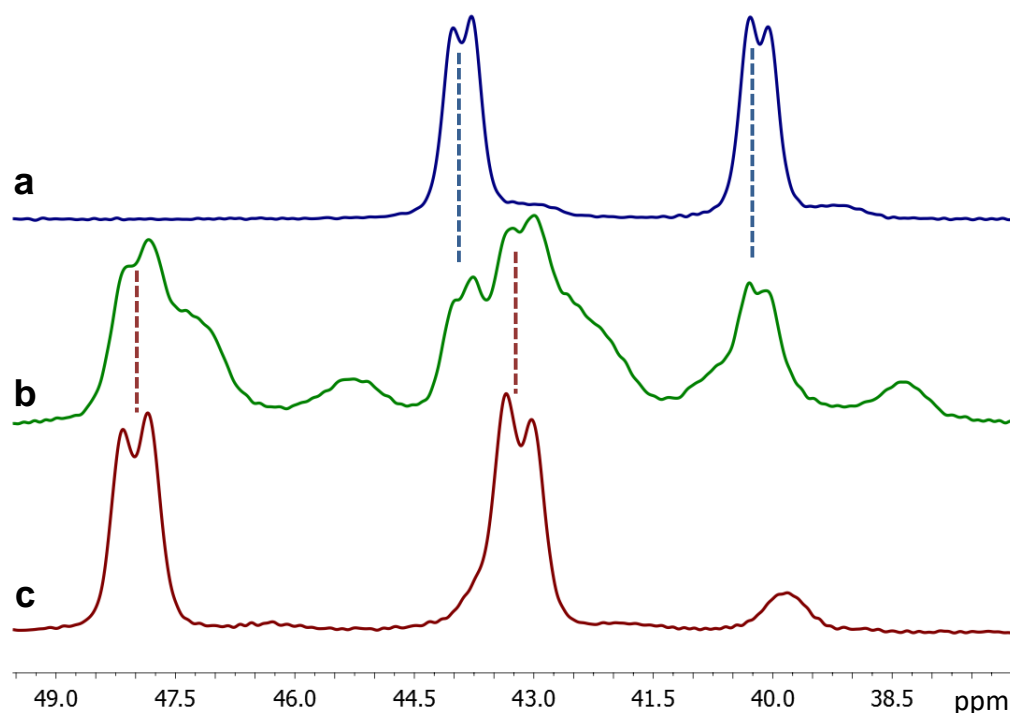
Figure 3. Solid state ^{31}P NMR spectra of complexes **1** (**a**) (see Fig. S24), **2** (**b**) (see Fig. S26 and for the deconvolution of this spectra see Fig. S27) and **4** (**c**) (see Fig. S25 in the ESI).

Deconvolution of the solid-state ^{31}P NMR spectrum recorded after fast evaporation of the liquor leading to complex **2** shows, therefore, that the spectrum corresponds to a mixture of mono-, di-, tri- and tetra- Ag complexes **1**, **2**, **3** and **4** in a relative proportion of 24, 19, 27 and 30 %, respectively (see Fig.S27 in ESI). This deconvolution analysis indicates that the solid-state ^{31}P NMR spectrum of complex **2** should be constituted by two pairs of doublets, where the signals corresponding to the two isotopes cannot be resolved, appearing at 42.77 ppm (10 %) [$^1J(Ag-^{31}P)$ = 750.00 Hz] and 40.67 ppm (9 %) [$^1J(Ag-^{31}P)$ = 754.21 Hz], respectively, (see Fig. S27 in the ESI) corresponding to the two different ^{31}P atoms present in the solid state in [(XPhos-

Ag)$_2$ μ_2-(η^4:η^2-COT)][SbF$_6$]$_2$ (**2**) (see ORTEP of complex **2** in Figure 1). In contrast to the solid-state ^{31}P NMR spectra, when pure complex [(XPhos-Ag)$_2$ μ_2-(η^4:η^2-COT)][SbF$_6$]$_2$ (**2**) is dissolved in CD$_2$Cl$_2$, only a single ^{31}P resonance is observed as commented earlier (see Fig. S13 in the ESI).

Curiously when this mixture of complexes **1**, **2**, **3** and **4** [Figure 3, bottom (**b**), for details see Figs.26-27 in the ESI] obtained by fast crystallization under reduced pressure of the crude dissolution of complex **2** was re-dissolved in CD$_2$Cl$_2$, no peaks besides those corresponding to the pure bis-Ag(I) [(XPhos-Ag)$_2$(μ_2-(η^4:η^2-COT)][SbF$_6$]$_2$ (**2**) complex at 43.54 ppm as a pair of doublets [$^1J(^{107}$Ag-^{31}P) = 626.59 Hz, $^1J(^{109}$Ag-^{31}P) = 723.63 Hz] were observed in the ^{31}P NMR spectrum recorded in solution, providing evidence that in solution the solid state mixture of complexes **1**, **2**, **3** and **4** [Figure 3, bottom (**b**)] is converted again into complex **2** (see Figs. S28-S29 for ^{1}H and ^{31}P NMR spectra in the ESI) with identical ^{1}H and ^{31}P NMR spectra as that of the pure crystallized sample of **2** (see Figs. S10 and S13 in the ESI). Single-crystal X-ray crystallography shows the formation from the mixture CH$_2$Cl$_2$/hexane (3/1) at -8 ºC of a polymorph structurally identical to complex **2** with a new coordination mode of COT with the two Ag ions in approximate by η^2:η^2 manner with adjacent "π" double bonds [(XPhos-Ag)$_2$ μ_2-(η^2:η^2-COT)][SbF$_6$]$_2$ (**2a**) (Table S3 and Fig. S30 in the ESI). The nearest carbon atoms of COT to the Ag1 atom (η^2 bonding form) are C41 and C42 of a double bond and the nearest carbon atoms of COT to the Ag2 atom (η^2 bonding form) are C47 and C48 of a double bond. NMR data of **2** in CD$_2$Cl$_2$ is consistent with fluxional behaviour of the COT ring even at -80 ºC where this exchange rate was not sufficiently slowed down at low temperature (See Figs. S31 and S32 in the ESI for ^{1}H and the ^{13}C{^{1}H} NMR spectra), indicating the fast exchange of Ag1$^+$ and Ag2$^+$ with the "π"-bonds of COT from C41=C42 and C45=C46 to C43=C44 and C47=C48 (see Figure 1, ORTEP of **2**).

Finally it was observed that, when non-dried solvents were used in the preparation or crystallization processes of Xphos-Ag(I)-(COT) complexes **1**, **2**, **3** or **4**, a partial hydrolysis occurs leading to the formation of a cationic aquo-Ag-Xphos complex (**5**) that could also be solved by single-crystal X-ray diffraction (see details in Table S4 and Fig. S33 in the ESI) revealing an identical structure to that recently published,[19] coinciding also the crystal structure with the polymorph previous reported.[12]

As it was mentioned at the beginning, activation of C-C bonds by transition metal complexes in homogeneous media is a constant area of research in organometallic chemistry.[23-28] In this context, it has recently been found the Ag(I)-mediated formation of a 2D cyano-bridged multinuclear Ag(I) alkynyl network formed throught the C-C bond cleavage of acetonitrile that is acting as source of CN$^-$ ions.[30] With the aim of gaining understanding on the activity of new cationic XPhos-Ag(I)-COT complexes as precursors of a new class of Ag clusters stabilized by bulky XPhos ligand, acetonitrile solutions of these complexes were submitted to photolysis. It was anticipated that, cyanide (CN$^-$) could also be generated by C-C bond cleavage of acetonitrile by complexes **1**-**4** and in this way the corresponding cyanide bridged Ag(I) complexes would be formed. Aimed at these goals, samples of complexes **1** and **4** in acetonitrile ($4 \cdot 10^{-4}$ M) were submitted to 266 nm laser irradiation (35 mW power), monitoring the changes in the optical absorption spectrum, as well as recording the corresponding transient absorption spectra (TAS), measuring the HRESI-MS and observing the formation of metal clusters by HR-TEM.

Upon photolysis, the UV-Vis spectra of both complexes **1** and **4** increases in intensity at 242, 325 and 466 nm [see Figure 4 (a) for complex **4** and for complex **1** see Fig.S34 in the ESI]. The absorbance at 242 nm coincides with that of phosphine ligand and the absorbance at 325 nm with that COT (see Fig.S35 in the ESI). Based on the observation of free ligands, the band centered at 466 nm is likely to correspond to the appearance of Ag clusters. The 466 nm absorption maximum is in accordance with previous studies[31-34] on DNA-templated Ag$_n$ clusters and monolayer-protected Ag clusters showing interband transitions between 400 and 600 nm.

TAS of complex **1** was recorded from 300 nm up to 600 nm at 5 µs delay after laser excitation at 266 nm. Subsequent spectra were monitored after prior submission of the acetonitrile solution of **1** to a number of laser pulses at 1 Hz [Figure 4 (b)]. The initial transient spectrum of complex **1** shows a main band centered at 380 nm and a shoulder at 460 nm. After laser exposure the main band was reduced and the shoulder at 460 nm grew into a new band increasing in intensity with the number of laser pulses [Figure 4 (b)]. Considering the coincidence of the 460 nm with the absorption of the plasmon band of Ag$_n$ clusters, it is proposed that the 380 nm band corresponds to an excited state of complex **1** that evolves giving rise to the formation of Ag$_n$ clusters. Transient kinetics were also recorded and they are presented in Figures S36-S39 of the ESI. The transient signal of complex **1** was recorded at 380 nm prior laser pulses while the temporal profile

of the solution containing cyano bridged multi nuclear Ag complexes after 320 laser shots was monitored at 460 nm (Figure S37 in the ESI). Both transient signal decays could be fitted to a two consecutive mono exponential kinetics $[f(t) = Y_0 + Ae^{-t/\tau_1} + Be^{-t/\tau_2}]$ with lifetimes τ_1: 3.23 µs and τ_2: 25.74 µs and τ_1: 4.05 µs and τ_2: 26.49 µs for the 380 nm and 460 nm signals, respectively.

The evolution of the transient signals at 380 nm and 460 nm corresponding to fresh complex **1** and the mixture of cyano bridged multi nuclear Ag complexes with laser irradiation are compared in Figures S35 and S36. As it can be seen there, the band centred at 380 nm corresponding to complex **1** decreases in signal amplitude with the number of laser pulses, indicating a decrease in the population of excited states of this transient species due to the decomposition of complex **1**. In contrast, the signal amplitude of the band appearing at 460 nm increases along irradiation indicating a growth in the concentration of the cyano bridged Ag complexes.

HR-TEM images of the clusters formed from a $4 \cdot 10^{-4}$ M solutions of complex **4** in acetonitrile were taken after irradiation with 360 and 720 laser shots at 35 mW power [Figure 4 (c) and (d), for details see in Figs. S40-S42 in the ESI]. No nanoparticles were observed for the solution of **4** before irradiation. After 360 shots the images of the irradiated sample show aggregated polydisperse nanobjects that should correspond according to HRESI-MS to $[(LAg)_2(\mu\text{-CN})_n(\mu\text{-Ag})_{n-1}]$ (n = 1, 2, 3 and 4) clusters [Figure 4 (c) and Fig. S40 in the ESI]. However upon prolonged irradiation, smaller and well dispersed nanoparticles are formed [Figure 4 (d) and Figs. S41-S42 in the ESI]. The elemental composition of these clusters was confirmed by EDX elemental mapping [Figure 4 (e) and Fig. S42 in the ESI).

The composition of these clusters as cyanide bridged di-, tri-, tetra- and penta- Ag clusters complexes was determined by HRESI-MS spectroscopy. Initially, and without laser irradiation, acetonitrile solutions of **1** or **4** show mainly a set of peaks with major positive MS peaks at 405.0692 and 407.0728 Da attributable to cationic XPhos-Ag(I) complex with the ^{107}Ag and ^{109}Ag isomers of $[C_{24}H_{31}AgF_6PSb$ (**1**) - SbF_6^- - COT$]^+$ (see Fig.S43 in the ESI) and a less intense set of peaks at 449.1265 Da attributable to cationic mononuclear silver acetonitrile XPhos-Ag-NCCH$_3$ complex (see Fig. S44 in the ESI). After laser exposure (90-360 shots at 35 mW) changes in the HRESI-MS were observed, appearing then a new set of peaks with major positive MS peaks at 838.1775 Da

attributable to cyanide bridged binuclear silver [XPhos-Ag]$_2$(CN)]$^+$ complex (see Figs. S45-S47 in the ESI). Also three new sets of peaks attributable to [(XPhos-Ag)$_2$(μ-CN)$_n$(μ-Ag)$_{n-1}$] (n = 2, 3 and 4), respectively, as bridged tri-, tetra- and penta- nuclear Ag complexes were recorded at 969.0915 (see Fig. S48 in the ESI), 1101.9996 (see Fig. S49 in the ESI) and 1234.9176 Da (see Fig. S50 in the ESI). The measured isotopic distribution for these cyanide bridged complexes [(XPhos-Ag)$_2$(μ-CN)$_n$(μ-Ag)$_{n-1}$] (n = 1, 2, 3 and 4) is in good agreement with the simulated isotopic distributions, for the molecular formula [C$_{41}$H$_{54}$Ag$_2$NP$_2$]$^+$, [C$_{42}$H$_{54}$Ag$_3$N$_2$P$_2$]$^+$, [C$_{43}$H$_{54}$Ag$_4$N$_3$P$_2$]$^+$ and [C$_{44}$H$_{54}$Ag$_5$N$_4$P$_2$]$^+$, respectively, (see details in Figs. S47-S50 in the ESI). The coincidence between the simulated and experimental isotopic distributions together with the high resolution mass of the peaks lend strong support to the corresponding molecular formulae and, therefore, to the existence of cyanide linkers.
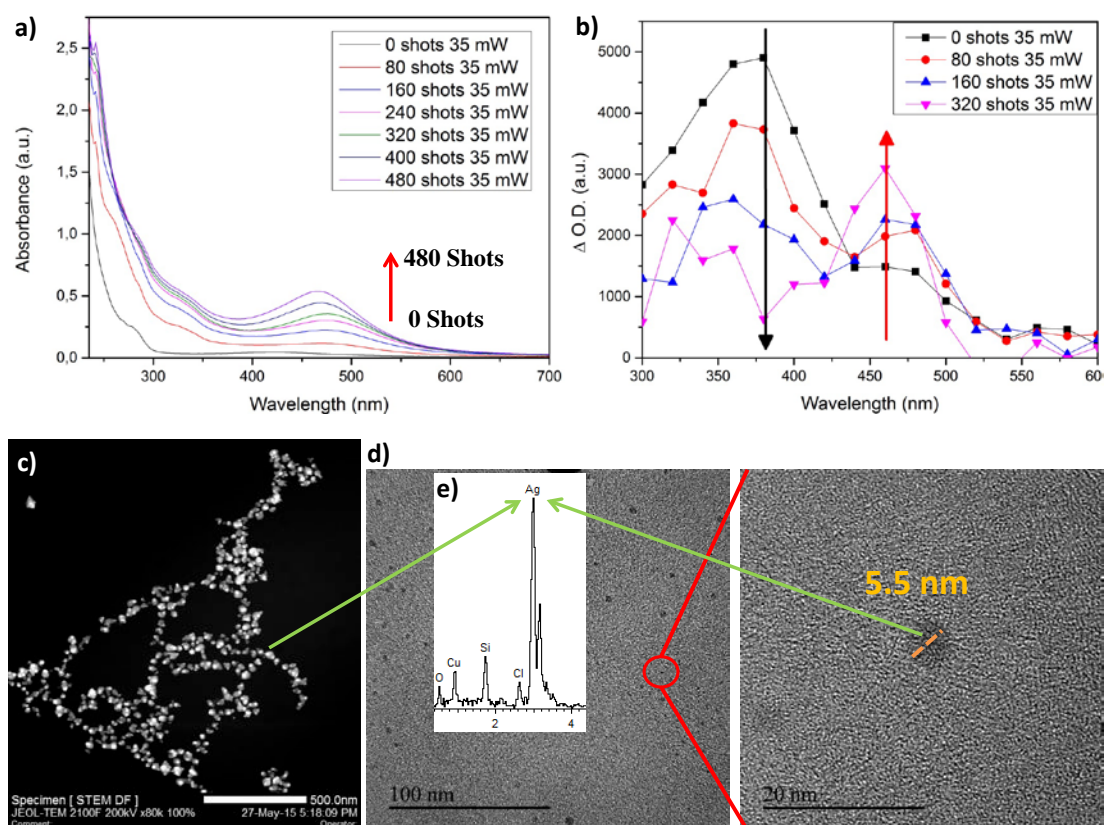
Figure 4. a) Temporal evolution of the UV/Vis spectra of 4.10^{-4} M acetonitrile solution of complex **4** upon irradiation with increasing number of laser shots as indicated in the figure. b) Transient spectrum of complex **1** monitored after different laser shots at 5 μs decay. c) HR-TEM images of an acetonitrile solution of complex **4** after 360 laser shots of 35 mW power. d) HR-TEM images of an acetonitrile solution of complex **4** after 720 laser irradiation shots at 35 mW. e) EDX spectrum of Ag clusters and nanoparticles.

In conclusion, a series of cationic single-, di-, tri- and tetra- Ag(I) π-complexes of COT with Buchwald-type phosphane have been synthetized and characterized. The solid state structure of the cationic mono- and di- Ag (I) XPhos π-complexes of COT ligand were resolved by single crystal X-ray crystallography revealing the coordination mode adopted by the COT ring in these complexes. Variable temperature NMR spectroscopy in CD_2Cl_2 reports on the fluxional behaviour of the COT ring. Upon light irradiation of XPhos-Ag(I)-COT complexes C-C bond cleavage of coordinated acetonitrile (XPhos-Ag(I)-NCCH$_3$) resulting in the formation of cyanide bridged Ag clusters was established by UV-Vis absorption spectroscopy and TEM. Information provided of HRESI-MS indicate that the transformation corresponds to the generation of defined small clusters up to 5 Ag atoms.

Experimental Section

Supporting information contains experimental details describing the preparation, isolation and full characterization of new silver complexes **1**, **2**, **3**, and **4** as well as silver complexes **2a** and **5**, including NMR spectra, combustion analysis, ESI-MS, HR-ESI-MS, HR-TEM, UV-VS, TAS and X-ray crystallography data. For cyclic voltammetry studies of complexes **1**, **2** and **4** see Fig. S51 in the ESI.

X-ray structure analysis data for: **1** (CCDC-1443116), **2** (1443117), **2a** (1443118) and **5** (1443119) contain full crystallographic data for this paper. These data can also be obtained free of charge from The Cambridge Crystallographic Data centre via http//www.ccdc.cam.ac.uk/data_request/cif.

1. T. Murahashi, S. Kimura, K. Takase, T. Uemura, S. Ogoshi and K. Yamamoto, *Chem. Commun. (Cambridge, U. K.)*, 2014, **50**, 820-822.
2. T. Murahashi, K. Usui, Y. Tachibana, S. Kimura and S. Ogoshi, *Chem. - Eur. J.*, 2012, **18**, 8886-8890, S8886/8881-S8886/8811.
3. T. Murahashi, E. Mochizuki, Y. Kai and H. Kurosawa, *J. Am. Chem. Soc.*, 1999, **121**, 10660-10661.
4. A. Grirrane, I. Resa, A. Rodriguez and E. Carmona, *Coord. Chem. Rev.*, 2008, **252**, 1532-1539.
5. R. Fernandez, A. Grirrane, I. Resa, A. Rodriguez, E. Carmona, E. Alvarez, E. Gutierrez-Puebla, A. Monge, J. M. Lopez del Amo, H.-H. Limbach, A. Lledos, F. Maseras and D. del Rio, *Chem. - Eur. J.*, 2009, **15**, 924-935.
6. O. T. Summerscales, X. Wang and P. P. Power, *Angew. Chem., Int. Ed.*, 2010, **49**, 4788-4790, S4788/4781-S4788/4786.
7. T. J. Kealy and P. L. Pauson, *Nature (London, U. K.)*, 1951, **168**, 1039-1040.
8. G. Wilkinson, M. Rosenblum, M. C. Whiting and R. B. Woodward, *J. Am. Chem. Soc.*, 1952, **74**, 2125-2126.
9. L. R. Moore, S. M. Cooks, M. S. Anderson, H.-J. Schanz, S. T. Griffin, R. D. Rogers, M. C. Kirk and K. H. Shaughnessy, *Organometallics*, 2006, **25**, 5151-5158.
10. M. L. Gallego, P. Ovejero, M. Cano, J. V. Heras, J. A. Campo, E. Pinilla and M. R. Torres, *Eur. J. Inorg. Chem.*, 2004, 3089-3098.
11. S. S. Y. Chui, M. F. Y. Ng and C.-M. Che, *Chem. - Eur. J.*, 2005, **11**, 1739-1749.
12. P. Perez-Galan, N. Delpont, E. Herrero-Gomez, F. Maseras and A. M. Echavarren, *Chem. - Eur. J.*, 2010, **16**, 5324-5332, S5324/5321-S5324/5156.
13. M. Israeli and L. D. Pettit, *J. Inorg. Nucl. Chem.*, 1975, **37**, 999-1003.
14. T. C. W. Mak, *J. Organomet. Chem.*, 1983, **246**, 331-339.
15. F. S. Matthews and W. N. Lipscomb, *J. Phys. Chem.*, 1959, **63**, 845-850.
16. H. Hosoya and S. Nagakura, *Bull. Chem. Soc. Jpn.*, 1964, **37**, 249-265.
17. D. Kim, S. Hu, P. Tarakeshwar, K. S. Kim and J. M. Lisy, *J. Phys. Chem. A*, 2003, **107**, 1228-1238.
18. D. S. Surry and S. L. Buchwald, *Angew. Chem., Int. Ed.*, 2008, **47**, 6338-6361.
19. A. Grirrane, E. Alvarez, H. Garcia and A. Corma, *Chem. - Eur. J.*, 2016, **22**, 340-354.
20. A. Grirrane, E. Alvarez, H. Garcia and A. Corma, *Angew. Chem., Int. Ed.*, 2014, **53**, 7253-7258.
21. A. Grirrane, E. Alvarez, H. Garcia and A. Corma, *Chem. - Eur. J.*, 2014, **20**, 14317-14328.
22. A. Grirrane, H. Garcia, A. Corma and E. Alvarez, *Chem. - Eur. J.*, 2013, **19**, 12239-12244.
23. F. L. Taw, A. H. Mueller, R. G. Bergman and M. Brookhart, *J. Am. Chem. Soc.*, 2003, **125**, 9808-9813.
24. Y. Zhu, M. Zhao, W. Lu, L. Li and Z. Shen, *Org. Lett.*, 2015, **17**, 2602-2605.
25. L. Li, C.-H. Wang, X.-L. Zhang and X. Liu, *Eur. J. Inorg. Chem.*, 2015, **2015**, 859-863.
26. T. Lu, X. Zhuang, Y. Li and S. Chen, *J. Am. Chem. Soc.*, 2004, **126**, 4760-4761.
27. D. S. Marlin, M. M. Olmstead and P. K. Mascharak, *Angew. Chem., Int. Ed.*, 2001, **40**, 4752-4754.
28. M. Tobisu, Y. Kita and N. Chatani, *J. Am. Chem. Soc.*, 2006, **128**, 8152-8153.
29. N. Hu, L. Gong, Z. Jin and W. Chen, *J. Organomet. Chem.*, 1988, **352**, 61-66.
30. K. Zhou, C. Qin, X.-L. Wang, L.-K. Yan, K.-Z. Shao and Z.-M. Su, *CrystEngComm*, 2014, **16**, 10376-10379.
31. T. U. B. Rao and T. Pradeep, *Angew. Chem., Int. Ed.*, 2010, **49**, 3925-3929, S3925/3921-S3925/3916.
32. Z. Wu, E. Lanni, W. Chen, M. E. Bier, D. Ly and R. Jin, *J. Am. Chem. Soc.*, 2009, **131**, 16672-16674.
33. I. Diez, M. Pusa, S. Kulmala, H. Jiang, A. Walther, A. S. Goldmann, A. H. E. Mueller, O. Ikkala and R. H. A. Ras, *Angew. Chem., Int. Ed.*, 2009, **48**, 2122-2125.

34. J. T. Petty, J. Zheng, N. V. Hud and R. M. Dickson, *J. Am. Chem. Soc.*, 2004, **126**, 5207-5212.